Caving 2026 – A van As, D Cumming-Potvin & J Wesseloo (eds)
© 2026 Australian Centre for Geomechanics, Perth, ISBN 978-1-7636842-3-2
doi:10.36487/ACG_repo/2645_46

Operational validity of the Es:Ep ratio for source mechanism classification in a block cave with a dense seismic network

Izak Gerhard Morkel [a,*]

[a] *IGM Geotechnical Pty Ltd, Australia*

Abstract

The ratio of S-wave to P-wave energy (Es/Ep) is a traditional parameter in mine seismology, used empirically to distinguish between shear and non-shear failure mechanisms. While moment tensor inversion (MTI) provides a far more complete physical representation of seismic sources, the Es/Ep parameter remains a practical tool for rapid assessment and back-analysis of historical catalogues. However, the reliability of standard Es/Ep thresholds is increasingly questioned due to inherent data quality challenges.

This paper evaluates the operational validity of the Es/Ep parameter by statistically comparing it against the automated MTI results from a densely seismically instrumented block cave mine. The Matthews correlation coefficient is used to assess classification confidence. Across the full catalogue, the standard thresholds gave a poor correlation, driven by a dominance of MTI shear events at low Es/Ep values. The MTI reference is itself automated and coverage-dependent, so the comparison measures agreement between 2 imperfect estimators, and the conclusions are conditional on the MTI being the more reliable of the 2.

Progressive filtering by the number of sensors used showed that strict sensor requirements raise the correlation to a reliable level, but at the cost of discarding the large majority of the dataset. Site-specific calibration restores diagnostic confidence yet leaves only a small fraction of events usable for single event analysis.

Keywords: *mine seismology, Es/Ep, Es:Ep ratio, seismic mechanisms, moment tensor inversion*

1 Introduction

The ratio of energy associated with the S-wave (Es) and P-wave (Ep) is dependent on the focal mechanism at the seismic source. In mine seismology, the Es:Ep ratio (or Es/Ep) is regarded as an important indicator of the type of failure occurring within the rock mass. Specifically, the parameter is used to distinguish between different source types, as the ratio is typically lower for tensile or non-shear events and higher for those involving fault slip or pure shear (Cai et al. 1998; Mendecki 2013).

In current mining seismology practice, the Es:Ep ratio is widely used for diagnostic purposes and to interpret rock mass response. Practitioners frequently employ this parameter to assign focal mechanisms to recorded events, relying on the assumption that the calculated values accurately reflect the source physics. Numerous studies have assigned diagnostic values to this ratio across various mining environments. Specific examples of its application include the assessment of interaction between open pit and underground developments, high-resolution seismic monitoring of open pit slopes, and the calibration of seismic hazard assessment tools using velocity fields and geotechnical data (Sweby et al. 2006; Reyes-Montes et al. 2010; Abolfazlzadeh et al. 2019).

Morkel et al. (2019) raised concerns regarding the usability of the Es/Ep parameter for routine seismic analysis. The calculation of this source parameter is highly sensitive to the introduction of systematic errors during waveform processing, with inconsistencies compounding across different seismic systems, algorithms, and human users. The historical confidence in assigning diagnostic value to the Es:Ep ratio for a single event

* Corresponding author. Email address: info@igmgeotechnical.com

has been shown to be problematic. However, it was also noted that confidence in the parameter could potentially be restored through further study detailing the specific conditions and assessment methods under which it remains reliable. Those investigations were carried out mainly in conventional stoping and open pit settings with relatively sparse seismic networks, which leaves open whether the parameter behaves differently in the denser networks typical of block caving.

Building on these findings, this study aims to determine whether useful information can still be extracted from the Es:Ep ratio and to explicitly define the operational conditions required to achieve this. If the parameter can be validated under specific constraints, this paper will further analyse the underlying reasons for the data inconsistencies identified in previous research. By isolating the physical and processing mechanisms involved in determining source mechanisms, we intend to better understand the reliability of the Es/Ep in mine seismology practice.

2 Background

2.1 Mine seismic network layout

In any seismic analysis, the geometry of the network relative to the recorded events shapes what can be resolved. This section sets out the geometry for the dataset used in this paper. Figure 1 shows a horizontal slice approximately 400 m thick through the dataset, with mine geometry and infrastructure omitted to keep the operator anonymous (the vertical sensor distribution is not shown but is broadly consistent through the cave). In a block cave, the network typically sits around and above the cave, so additional sensors mainly extend the coverage from one side rather than around the full focal sphere. A full 360° coverage of the source is unlikely for most events, and the practical aim is closer to 180°. Events located between the sensors and the cave, and events located behind the sensors relative to the cave, gain similar one-sided coverage from this layout.

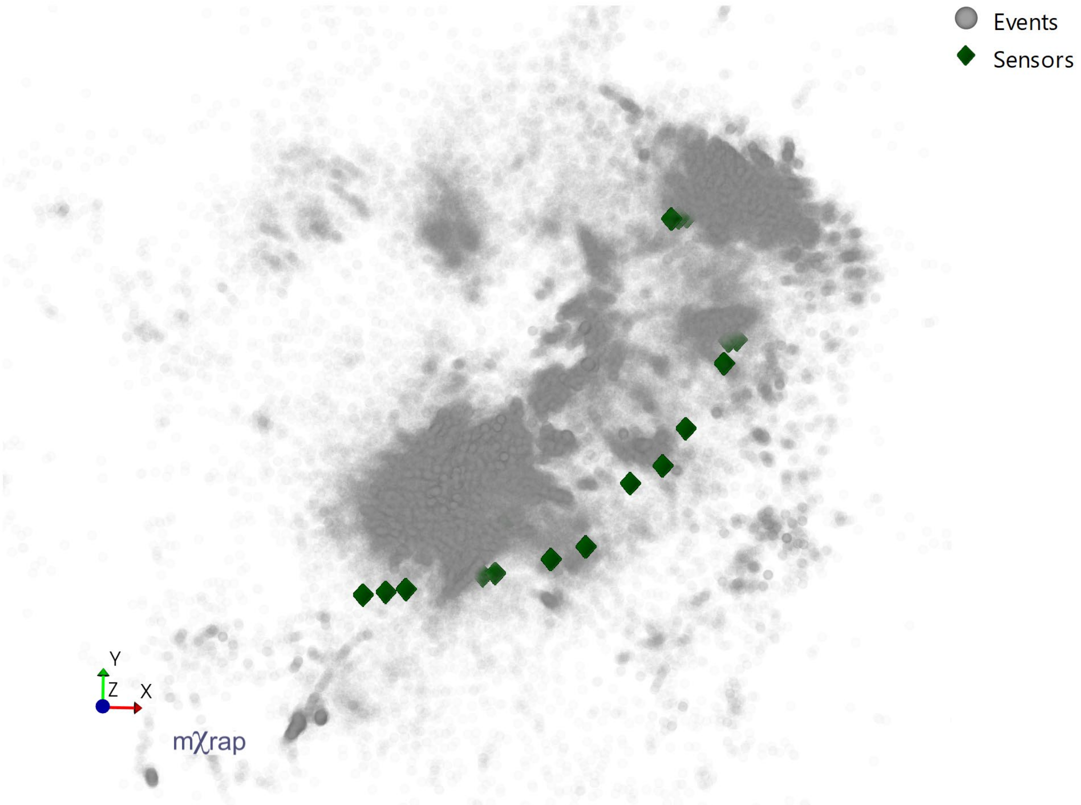

Figure 1 Horizontal slice through the dataset showing the location of sensors (green diamonds) relative to the seismic events (grey). Mine geometry and infrastructure are omitted to keep the operator anonymous

Ma et al. (2018) demonstrated that 2 factors are central to resolving the focal mechanism: the three-dimensional sensor coverage of the source, and the signal-to-noise ratio at the recording sensors. Our analysis does not isolate these factors directly. Instead, the used sensor count is used as a proxy for both the factors raised by Ma et al. (2018). More used sensors generally translate to better source coverage in caving networks, and to a more constrained moment tensor inversion (MTI). A high used sensor count is also an indicator of event magnitude, since larger events exceed the trigger threshold at more sensors; larger events are expected to record at higher signal-to-noise on average, although this has not been verified for the present dataset.

2.2 Es:Ep ratio

Based on the theoretical partition of radiated seismic energy, Sato (1978) demonstrated that tensile failure models produce approximately equal S-wave and P-wave energies. Conversely, pure shear events generate considerably larger S-wave energy, typically resulting in an Es/Ep greater than 20. This theoretical foundation has been translated into a diagnostic convention, summarised in Table 1, which categorises source mechanisms based on discrete threshold values. For instance, Gibowicz et al. (1991) and Gibowicz & Kijko (1994) suggest that ratios below 10 indicate the presence of a tensile failure component, while Boatwright & Fletcher (1984) associate values greater than 10 with pure shear. Hudyma & Potvin (2010) classify events with an Es:Ep ratio of less than 3 as non-shear mechanisms. To accommodate the wide dynamic range of seismic energy, these threshold values are also frequently evaluated in the logarithmic domain, log(Es:Ep ratio).

Table 1 Interpretation of Es:Ep ratio threshold generally used in the mining industry

Es:Ep ratio threshold	Log(Es:Ep ratio) threshold	Mechanism interpretations
<1	<0.0	Pure tensile
1–3	0–0.5	Non-shear
3–10	0.5–1.0	Mixed
>10	>1.0	Shear

Many of the foundational studies establishing these threshold limits rely on generalised or highly curated datasets to demonstrate optimal correlation. However, routine seismic data processing is complex, and standard catalogues frequently suffer from numerous data quality issues and systematic shifts (Morkel et al. 2015; Morkel & Wesseloo 2017). It must therefore be assumed that these inherent data quality challenges will directly impact the reliability and interpretation of the Es/Ep parameter in practice. The application of rigid thresholds is likely flawed. Operations with higher uncertainty in their seismic catalogues may require more conservative threshold limits to ensure accurate source mechanism interpretation, whereas mines maintaining well-curated catalogues could apply more aggressive thresholds without reducing the predictive reliability of the Es:Ep ratio. The operational objective should be to determine site-specific Es/Ep thresholds that optimise the volume of usable seismic events while maintaining the confidence and reliability of the interpretations above an acceptable standard.

It may be argued that the diagnostic utility of the Es:Ep ratio has diminished with the rapid advancement and automation of moment tensor inversion (MTI) techniques. Given the decreasing cost of computational power, it is increasingly preferable for most seismic events to undergo MTI processing to obtain an understanding of the source mechanism. While it is our opinion that the relative value of the Es:Ep ratio has decreased in recent times, it remains a standard source parameter universally available in almost all historical and contemporary seismic catalogues.

Therefore, provided the operational conditions under which the parameter is accurate are well understood, the Es:Ep ratio retains several highly practical applications in mine seismology. Firstly, it allows practitioners to conduct detailed back-analyses of historical datasets where MTI data is unavailable, thereby enriching the geotechnical context of past instability. Secondly, because the Es:Ep ratio is calculated immediately upon routine waveform processing, it provides a rapid preliminary assessment of the likely source mechanism during time-sensitive or emergency situations. Finally, in operational environments where MTI processing is prohibitively expensive or time-consuming, a well-calibrated Es:Ep ratio assessment serves as a cost-effective alternative for populating the database and evaluating broader rock mass response trends.

2.3 Moment tensor inversion

MTI is a well-established analytical technique that provides a full mathematical representation of the equivalent forces acting at a seismic source. Unlike the empirical Es:Ep ratio, which provides a simplified scalar proxy to distinguish between shear and non-shear events, MTI explicitly decomposes the rock mass response into its volumetric and deviatoric components (Vavryčuk 2015). This physical description allows practitioners to accurately identify complex mixed-mode failure mechanisms, including varying degrees of implosion, explosion, and pure shear. In this study, MTI serves as the theoretical ground truth against which the reliability and diagnostic validity of the Es:Ep ratio parameter can be systematically evaluated.

To interpret and communicate the complex three-dimensional source mechanisms derived from MTI, practitioners rely on specialised source-type diagrams. The Hudson plot, originally developed by Hudson et al. (1989), maps the full moment tensor onto a two-dimensional domain. This plot geometrically separates the mechanism into a pure double-couple (shear) at the centre, purely isotropic (explosive or implosive) components at the vertical poles, and compensated linear vector dipoles along the horizontal axis. Building on these visualisations, the diamond plot is an alternative representation of the same decomposition, with the source-type regions and boundary lines laid out differently (Vavryčuk 2015). These graphical tools are standard for enabling a direct visual comparison with the empirical thresholds traditionally assigned to the Es:Ep ratio.

To make MTI data easier to practically interpret, theoretical boundaries can be overlaid on source-type plots to group events by their primary failure mechanism. Rigby (2024) defined physical limits to assess whether a seismic event can be broken down into basic geotechnical processes. These processes include rock mass shear, convergence-driven crushing (closing cracks), or blast-type expansion (opening cracks). As shown by the black lines in Figure 2, these boundaries divide the plot into distinct zones for shear-type, crush-type, and blast-type mechanisms. The exact position of these lines depends on the elastic properties of the rock mass, specifically the Poisson's ratio, which is set to 0.25 in this instance.

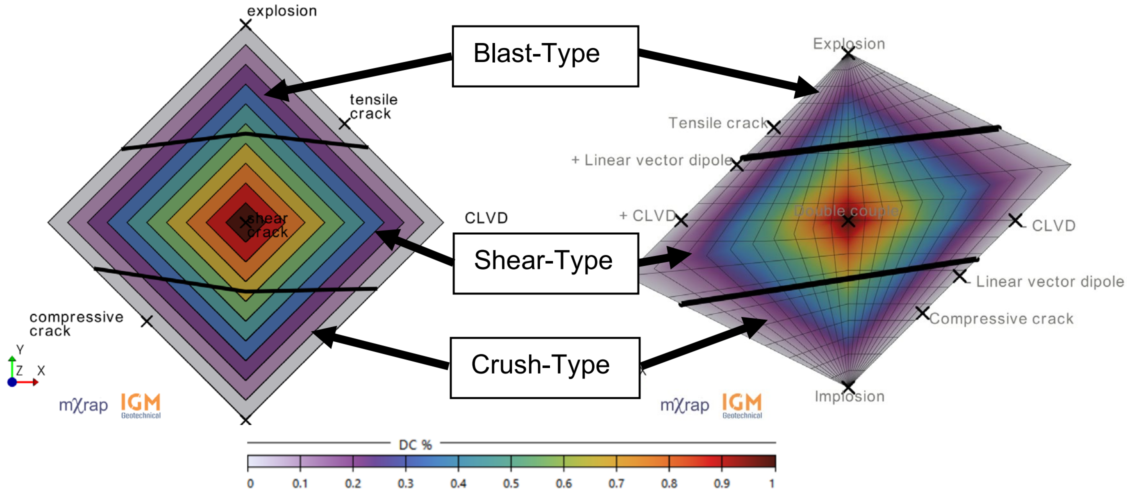

(a) (b)

Figure 2 (a) Diamond and (b) Hudson source-type plots illustrating the theoretical mechanism boundaries (black lines) defined by Rigby (2024). The delineated regions categorise events into blast-type, crush-type, and shear-type mechanisms, assuming a rock mass Poisson's ratio of 0.25. Mechanism areas are coloured according to their calculated double-couple percentage

While the theoretical boundaries established by moment tensor decompositions provide a mathematical framework, it must be acknowledged that MTI is not an absolute ground truth. Much like empirical Es:Ep ratio thresholds, MTI relies on specific physical assumptions that do not fully capture the chaotic reality of a fracturing rock mass. In practice, seismic wave propagation is highly complex; ray paths are rarely straight, and seismic velocities vary significantly due to lithological heterogeneity, induced fracturing, and the presence of mining voids. Mismodelling these velocity structures directly impacts the accuracy of the calculated event origin, which in turn introduces errors into the MTI process. The stability and accuracy of the inversion are highly dependent on the three-dimensional spatial coverage of the sensor network, the total number of available sensors used, and the signal-to-noise ratio. Ma et al. (2018) demonstrated that even minor inaccuracies in source coverage or moderate levels of seismic noise can introduce significant artificial shifts on a mechanism plot, generating spurious isotropic components as inversion artefacts. Compounding errors throughout the measurement and processing chain mean that individual MTI solutions contain inherent uncertainty.

The dataset for this study consists of automatically processed MTI solutions from a single seismic system at a single block cave operation. The choice of dataset is driven by 2 practical constraints that frame how the conclusions should be read.

First, the analysis requires a large MTI catalogue. The Es:Ep ratio is tested against the MTI classification on an event-by-event basis, and meaningful statistical separation of shear and non-shear populations relies on a population of the order of thousands of events with MTI solutions. From our experience, no operation routinely produces a manually processed, expert-reviewed MTI catalogue of this size. Manual MTI processing of even a few hundred events is a substantial undertaking, and a manually processed catalogue exceeding 1,000 events is, to the author's knowledge, not available at any site. Automated MTI processing is the only practical source of the data volumes required for this kind of analysis.

Second, the analysis depends on high sensor counts. The hypothesis being tested is that the predictive quality of the Es:Ep ratio improves with the number of used sensors. Testing that hypothesis requires a network with enough sensors that filtering down to subsets of over 60 sensors still leaves a usable population. Block cave operations have, on average, the densest seismic networks available and are therefore the most suitable mining environment for this work.

Given these constraints, the automated MTI results are adopted as the working ground truth against which the Es:Ep ratio is tested. We assume that the error margin on automated results is higher than on manually processed solutions, but that the errors are systematic rather than random because automated processing applies consistent algorithms. The implications of this choice for the scope of the conclusions are addressed in Section 5.

3 Methodology

The Es/Ep parameter quality were checked prior to the analysis. Events with Es/Ep recorded as 1.0, which is the flag for cases where either Es or Ep could not be calculated, were found to have a minimal impact on the results. From our previous work, the broader assumption of MTI data quality cannot be made blindly (Morkel et al. 2015; Morkel & Wesseloo 2017), but any database-level deviation will surface as anomalies in the results and is addressed in Section 5.

The approach taken in this study relies on the assumption that the MTI results, when categorised according to the physical boundaries suggested by Rigby (2024), represent a ground truth for source mechanisms. To achieve this, the investigation is structured as a binary prediction analysis, statistically evaluating whether the empirically assigned Es:Ep ratio class correlates with the corresponding MTI mechanism class. For the purposes of this binary assessment, the MTI blast-type and crush-type mechanisms are combined into a single non-shear class. Events with an Es:Ep ratio below 3 are predicted as non-shear, whilst events with a ratio above 10 are predicted as shear (Figure 3). Events falling within the intermediate mixed zone (Es:Ep ratio between 3 and 10) are not considered and explicitly excluded from the statistical assessment.

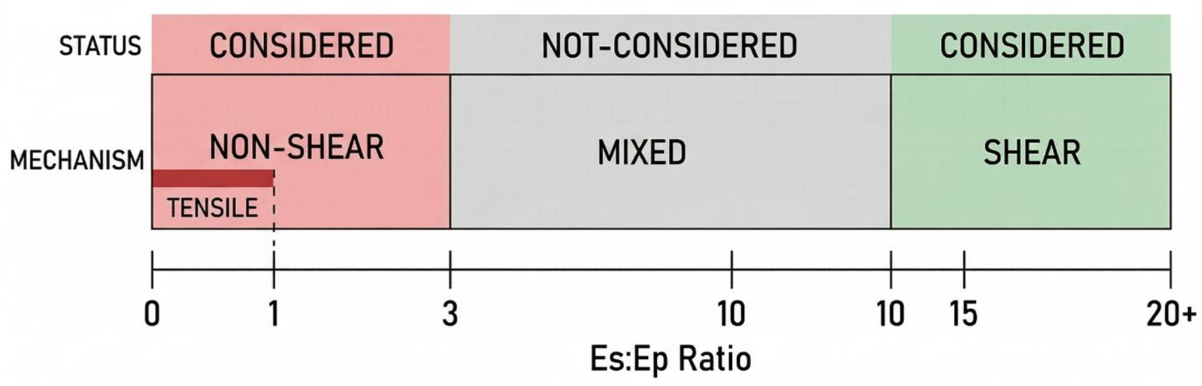

Figure 3 Conceptual framework for discretising the Es:Ep ratio into binary mechanism classes for comparative analysis. Tensile mechanisms are shown for reference and are not included in the binary shear/non-shear evaluation undertaken in this study

To determine the specific circumstances under which the Es:Ep ratio can be used as an accurate proxy for the mechanism classes obtained from MTI, this study evaluates the impact of the number of sensors used on parameter reliability. Following a baseline analysis of the complete dataset, the methodology involves systematically excluding seismic events recorded by a lower number of sensors. The core hypothesis is that if the Es:Ep ratio's utility in correctly predicting shear and non-shear mechanisms improves as the number of used sensors increases, it would demonstrate that the parameter could remain operationally useful under well-constrained monitoring conditions. By quantitatively evaluating the predictive confidence of the Es/Ep parameter across different sensors used thresholds, this analysis aims to define practical, data-driven limits for when the ratio can be applied with greater confidence in routine geotechnical practice.

If the predictive accuracy of the Es:Ep ratio demonstrates a strong improvement as the number of used sensors increases, the subsequent objective of this research is to actively optimise its operational application. Therefore, the study will systematically evaluate combinations of minimum sensor counts and Es/Ep thresholds to identify the ideal operational balance: achieving a strong, reliable predictive correlation against the MTI ground truth while simultaneously maximising the total volume of events retained for geotechnical analysis.

4 Analysis

4.1 Baseline statistical analysis

The statistical analysis investigates the dataset to understand how the distribution of shear and non-shear events varies with the calculated Es:Ep ratio. The primary metrics considered are the percentages of events accurately predicted as shear and non-shear. These percentages serve as a confidence metric for the empirical thresholds. To further evaluate the predictive correlation of the Es/Ep parameter against the MTI ground truth, a standard confusion matrix is generated to categorise the binary classification results into true and false predictions (Fawcett 2006). From this matrix, the Matthews correlation coefficient (MCC) is calculated to provide a balanced metric of the overall predictive performance (Matthews 1975).

A comparative analysis was conducted on a catalogue of 64,925 seismic events possessing both MTI solutions and calculated Es:Ep ratios. Applying the standard Es/Ep thresholds, the dataset was partitioned into 25,538 shear events, 9,239 non-shear events, and 30,148 mixed events. The unexpectedly high proportion of mixed events, comprising nearly half of the analysed dataset, highlights how much data is left on the table with the standard Es/Ep threshold limits. Figure 4 illustrates the source-type mechanisms for this baseline dataset, plotting only the events explicitly classified by their Es/Ep thresholds as shear (red) and non-shear (blue). The solid black lines represent the theoretical boundaries defined by Rigby (2024), which separate the MTI shear and non-shear classes.

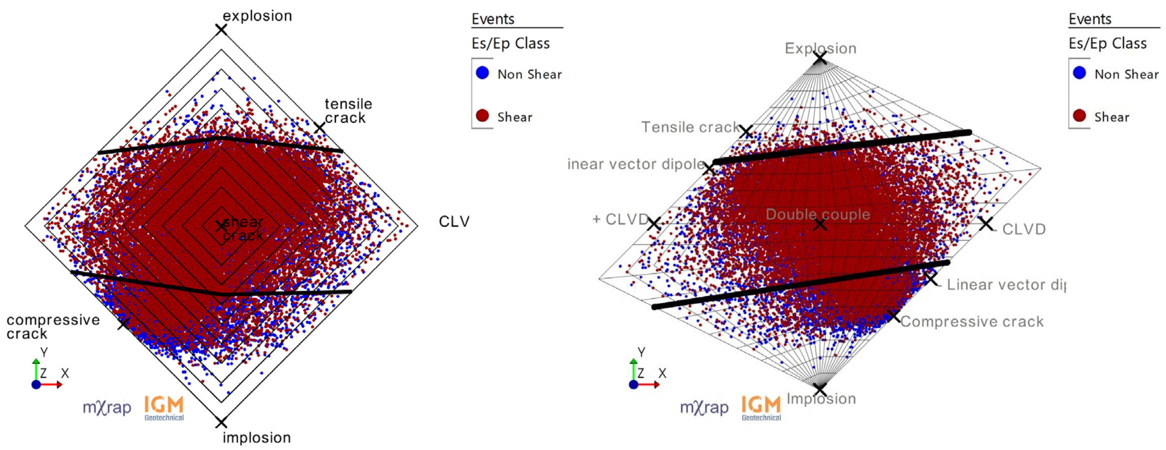

(a) (b)

Figure 4 (a) Diamond and (b) Hudson source-type diagrams for the subset of events that received an moment tensor inversion solution and were classifiable under the Es/Ep thresholds (red = shear, blue = non-shear). The solid black lines mark the theoretical shear/non-shear boundaries from Rigby (2024)

Figure 5 presents a stacked distribution plot designed to illustrate the underlying mechanism properties of the baseline dataset. By observing these stacked, binned bars, where red represents MTI-defined shear and blue represents non-shear, the proportion of non-shear events increases as the Es/Ep decreases, while the proportion of shear events increases as Es/Ep rises. This trend aligns with theoretical expectations. However, an evaluation of the conventional thresholds reveals some clear concerns. Ideally, the target mechanism should dominate its respective domain. For the shear threshold (Es/Ep > 10), this holds reasonably true, with shear events constituting over 85% of the data in most bins above this limit. Conversely, the non-shear threshold (Es/Ep < 3) performs poorly, capturing a non-shear component of only ~30% within those lower bins. This illustrates the inadequate predictive accuracy for non-shear events using the standard Es/Ep threshold limit.

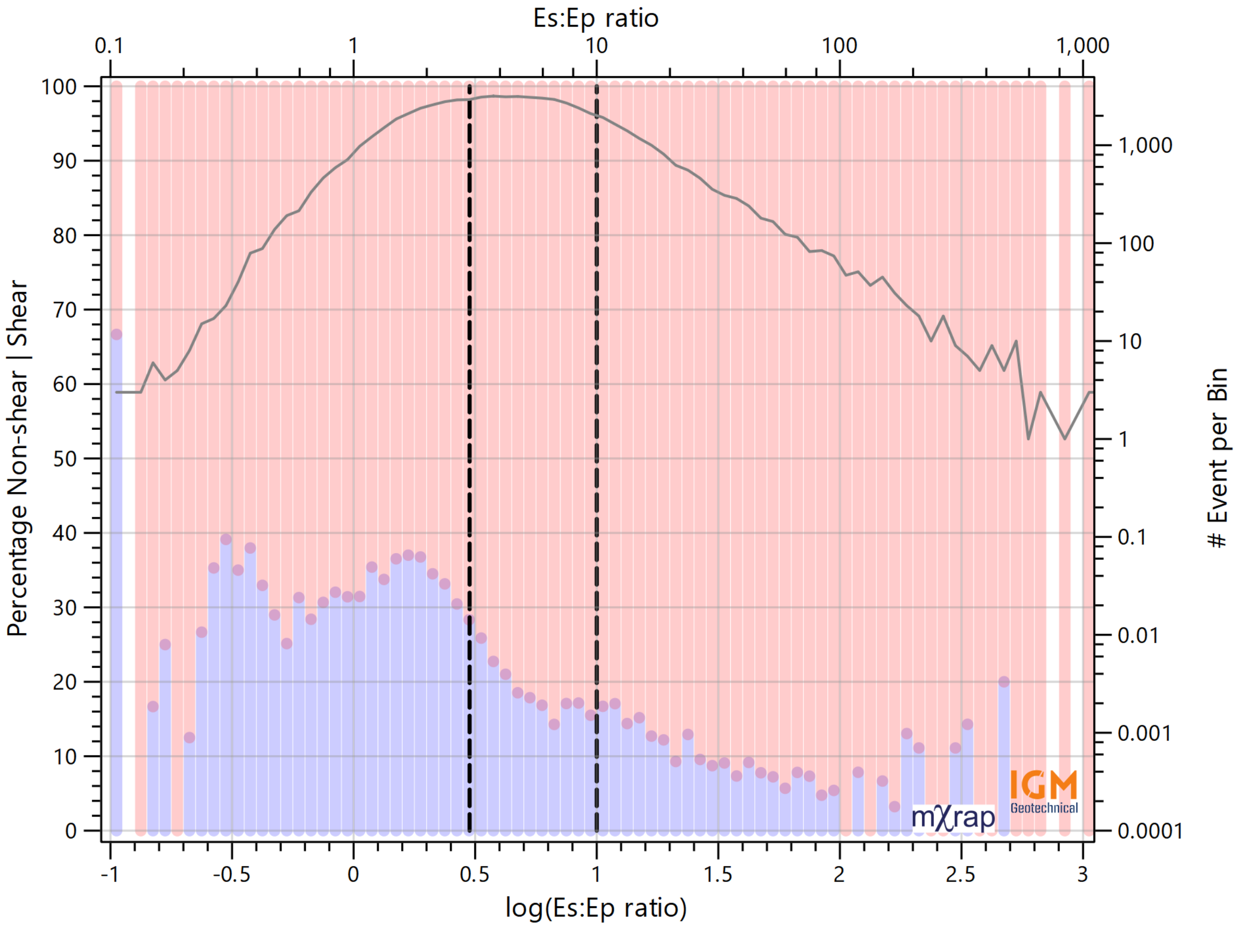

Figure 5 **Stacked plot displaying the percentage of moment tensor inversion defined shear and non-shear mechanisms distributed across Es:Ep ratio bins. The red component of the stacked bars indicates the proportion of shear-type events, whereas the blue component represents non-shear-type events. The total number of events within each bin is denoted by the solid grey line, plotted against the secondary y-axis. The standard empirical Es/Ep thresholds are indicated by the vertical dashed lines, representing Es/Ep = 3 for the suggested non-shear boundary and Es/Ep = 10 for the suggested shear boundary**

To further evaluate the predictive capability of the empirical thresholds, the dataset is described using cumulative distribution functions (CDFs), as presented in Figure 6. This standard analytical approach in engineering practice allows practitioners to rapidly determine classification accuracy and confidence levels at any specific Es/Ep threshold value. For instance, observing the shear CDF (red curve), it is established that approximately 77% of the total dataset consists of MTI-defined shear events. When applying the standard operational threshold of Es/Ep > 10, the predictive accuracy is roughly 86%, meaning that nearly 9 out of 10 events predicted as shear using this limit will correctly align with the MTI mechanism. Conversely, the non-shear CDF (blue curve, cumulating from large to small Es/Ep values) indicates that non-shear events comprise approximately 23% of the total database, and at the standard non-shear threshold of Es/Ep < 3, the confidence level reaches only about 33%. Practically, this means that only 3 out of every 10 events predicted as non-shear are accurately identified by the MTI ground truth, representing a poor diagnostic return.

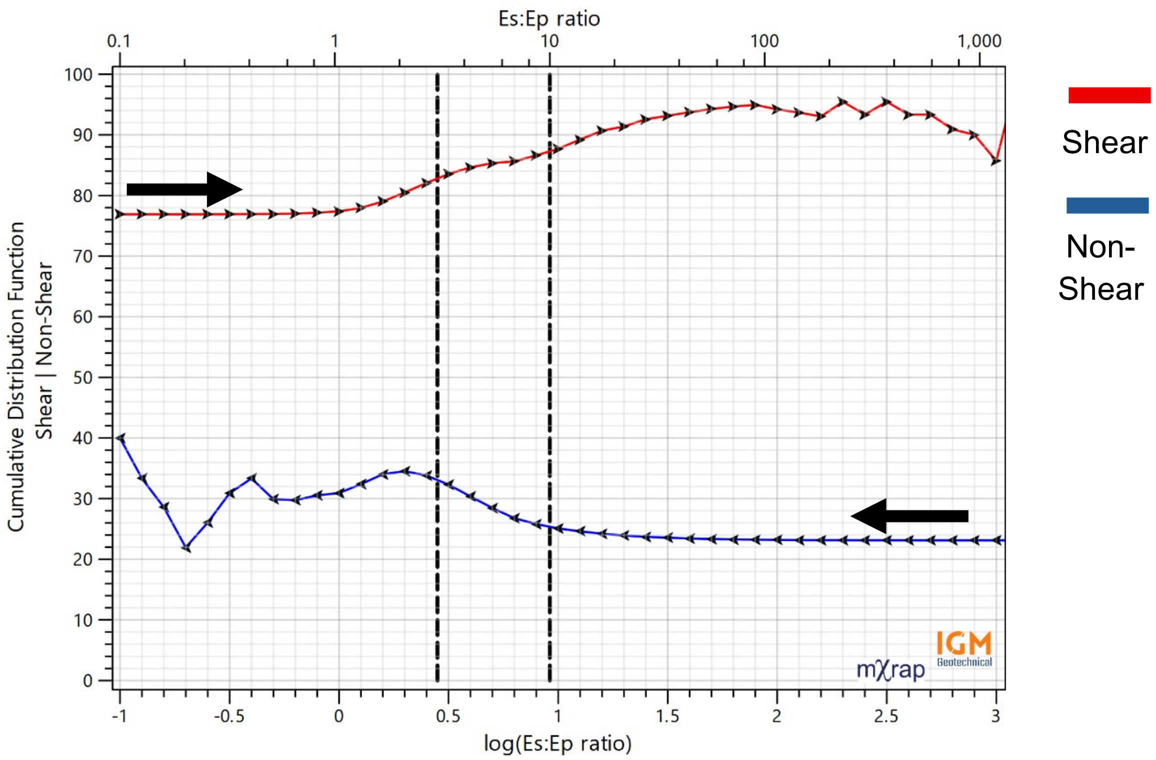

Figure 6 **Cumulative distribution function of the moment tensor inversion defined shear (red curve) and non-shear (blue curve) data plotted against the Es:Ep ratio. The arrows along the curves denote the direction of data cumulation (black arrows). The vertical dashed lines indicate the standard empirical thresholds at Es/Ep = 3 and Es/Ep = 10**

This combined evaluation is necessary because adjusting the thresholds in isolation can be misleading. For example, arbitrarily decreasing the shear Es/Ep threshold to 1 would artificially capture almost all MTI-defined shear events, but it completely obscures the parameter's inability to separate shear from non-shear mechanisms. The confusion matrix (Fawcett 2006) overcomes this limitation by assessing all possible binary classification outcomes to determine the true quality of the prediction:

- True positive: events correctly predicted as shear
- True negative: events correctly predicted as non-shear
- False positive: events incorrectly predicted as shear
- False negative: events incorrectly predicted as non-shear.

To consolidate these 4 outcomes into a single, reliable performance metric, the MCC is used (Matthews 1975). The MCC is useful for evaluating binary classifications because it accounts for heavily imbalanced datasets, such as the shear-dominated catalogue analysed in this study. It produces a high score only if the prediction obtained good results across all 4 matrix categories. The resulting MCC values are interpreted according to the standard ranges outlined in Table 2.

Applying this statistical framework to the baseline results shown in Figure 7, the standard thresholds perform poorly. The high volume of actual shear events incorrectly dominating the lower Es/Ep ranges, represented by the large number of false negatives (15,148 events), severely degrades the parameter's overall predictability. This results in an MCC value of 0.22, which classifies the predictive relationship as a weak correlation. This value lies barely above the 0.20 threshold, indicating that the standard Es/Ep boundaries provide a classification capability that is only marginally better than a random guess and offer very little practical diagnostic value.

Table 2 Matthews correlation coefficient score ranges and interpretations.

Score range	Interpretation	Description
0.70–1.00	Strong correlation	The classifier is highly reliable and accurately predicts the target mechanism
0.40–0.70	Moderate correlation	A clear trend exists, though there is some overlap or noise in the prediction
0.20–0.40	Weak correlation	The classification is only slightly better than a random guess
-0.20–0.20	No correlation	The parameters provide no predictive power for the chosen mechanism
Less than -0.20	Inverse correlation	The classifier is consistently predicting the opposite of the ground truth

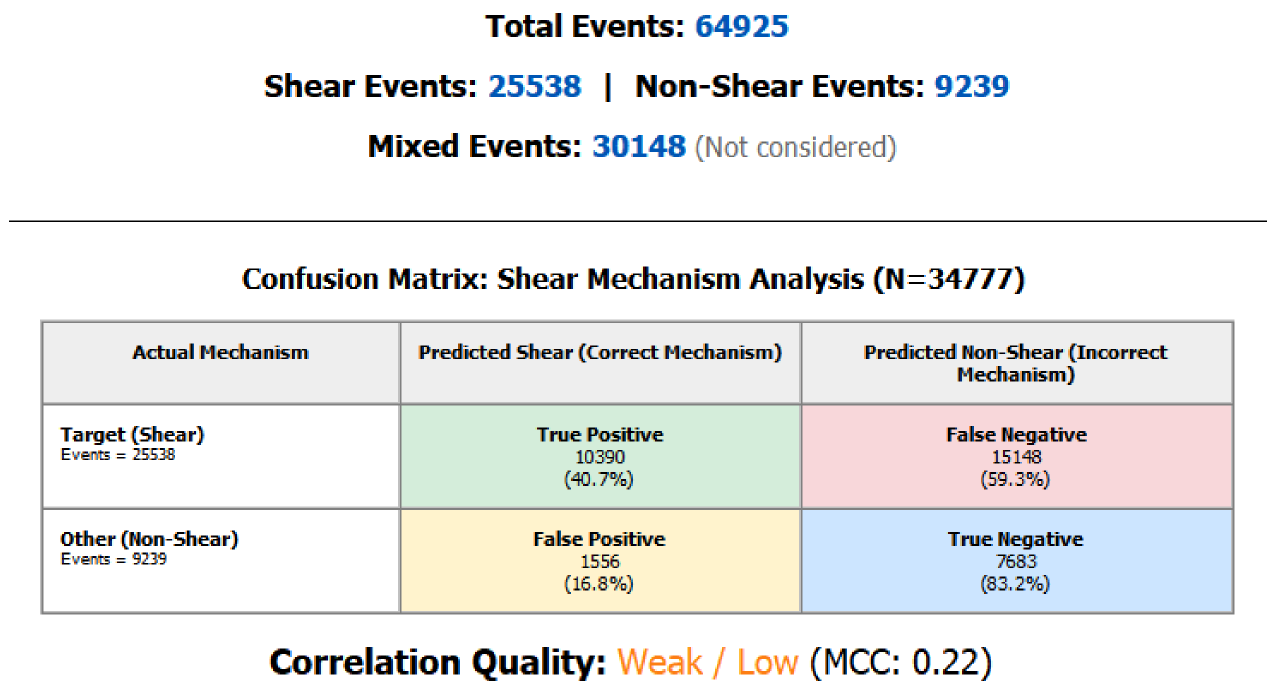

Figure 7 Confusion matrix detailing the binary classification performance of the standard Es/Ep thresholds against the moment tensor inversion defined baseline. The overall predictive correlation is evaluated as weak, denoted by a Matthews correlation coefficient (MCC) of 0.22

This baseline analysis shows a poor correlation, driven by the dominance of MTI shear events at low Es/Ep values and the resulting high false negative count. The high proportion of MTI shear, about 77%, may also point to systematic biases in the automated MTI processing.

Nevertheless, these baseline results corroborate the conclusions of Morkel et al. (2019), confirming that applying standard Es/Ep thresholds indiscriminately across an entire database, even within a densely instrumented cave mine, yields unreliable results. While previous research advised against relying on this parameter for isolated single events, this analysis extends that caution, demonstrating that it is equally unreliable when applied broadly to groups of events. The question remains whether isolating specific operational conditions, such as restricting the analysis based on the number of used sensors, can improve the statistical reliability of the Es:Ep ratio to a point where the parameter becomes practically usable.

4.2 Impact of sensors used

In this section, the predictive properties of the dataset are evaluated across 3 progressively restrictive scenarios, namely more than 20, 40, and 60 sensors, respectively. Throughout these scenarios, the standard Es/Ep thresholds are maintained. The primary objective is to determine the extent to which the statistical predictability of the Es:Ep ratio improves as sensor count improves (a proxy for network coverage). Concurrently, this section assesses the trade-off between increased classification accuracy and data retention.

Filtering to events recorded by more than 20 sensors reduces the catalogue from 64,925 to 11,155 events (an 83% decrease), but the predictive characteristics of the remaining data improves. In the stacked plot (Figure 8, top left), the non-shear component below Es/Ep 3 is more pronounced than in the baseline, and the diamond diagram (top right) shows better separation between mechanism types, though some events remain misclassified. The CDFs (Figure 8, bottom left) show the shear proportion (Es/Ep > 10) is around 88% and non-shear (Es/Ep < 3) around 55%. The MCC rises to 0.36, still within the weak correlation range.

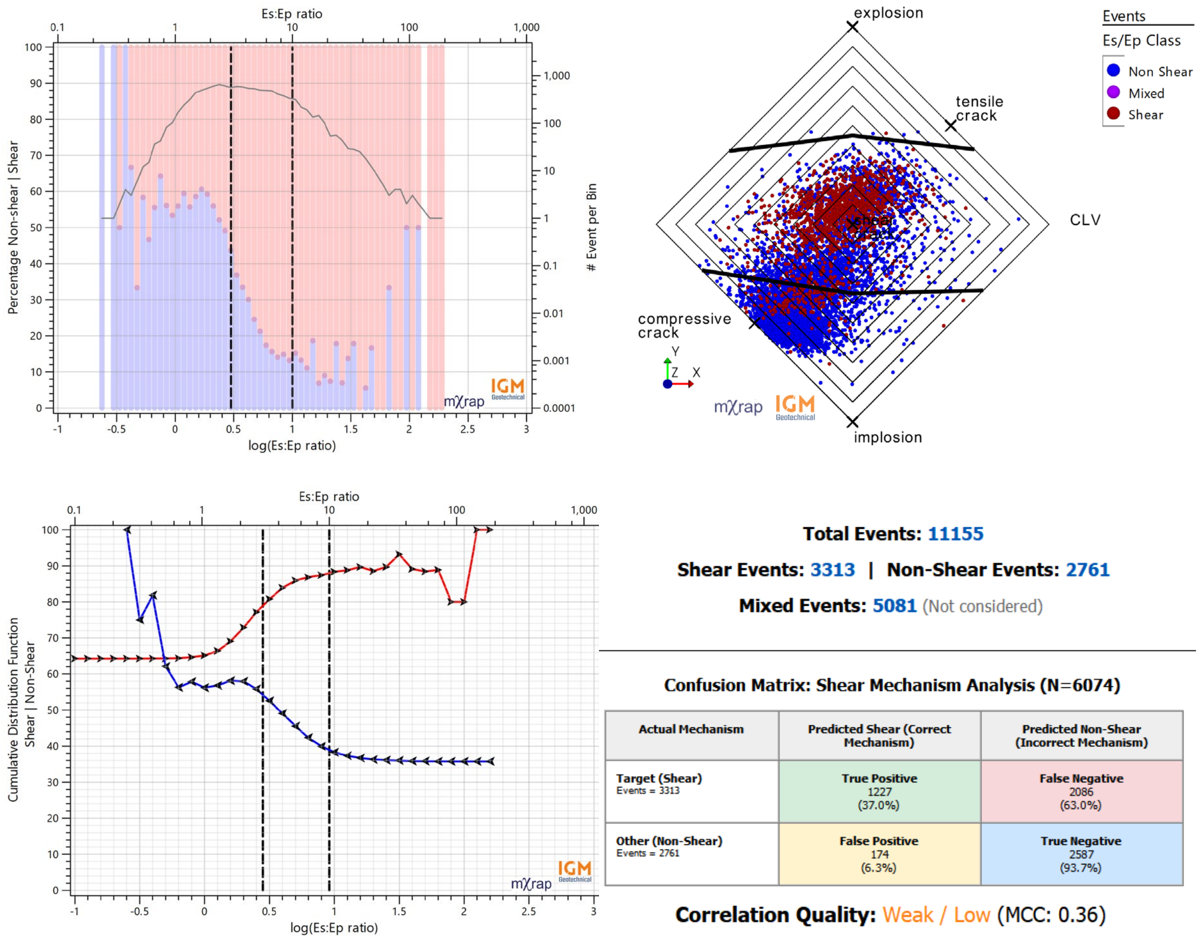

Figure 8 Evaluation of the filtered dataset comprising seismic events processed with more than 20 sensors. The subplots display the stacked distribution of mechanisms across Es/Ep bins (top left), the diamond diagram (top right), the cumulative distribution functions for the filtered data (bottom left), and the resulting confusion matrix, which yields an improved Matthews correlation coefficient (MCC) of 0.36 (bottom right)

Filtering to more than 40 sensors reduces the catalogue to 3,700 events (a 94% decrease). In the stacked plot (Figure 9, top left), the non-shear component below Es/Ep 3 now accounts for 80% or more, and the diamond diagram (top right) shows good separation, with few events misclassified. The CDFs (Figure 9, bottom left) show the shear threshold accuracy reaches about 95% and non-shear about 75%, raising the MCC to 0.59, now in the moderate correlation range.

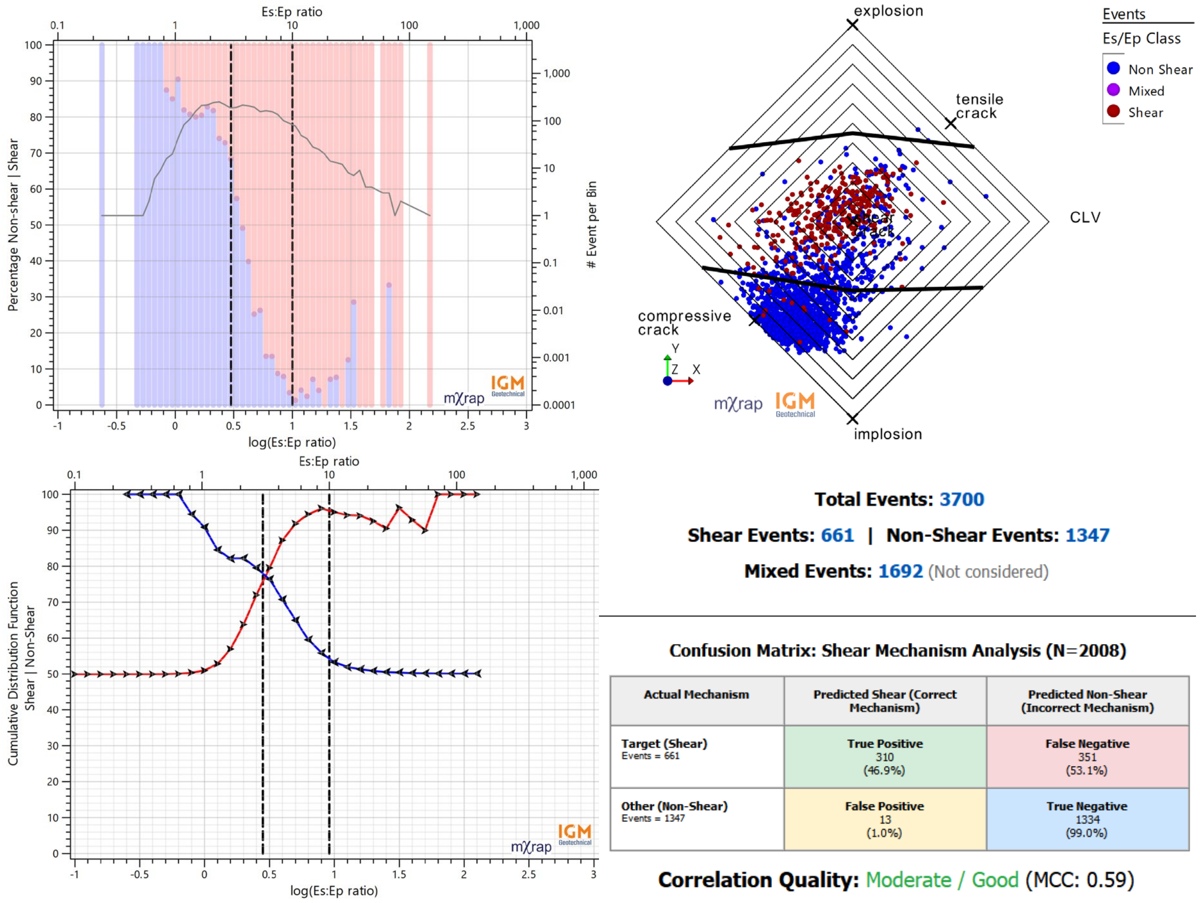

Figure 9 Evaluation of the filtered dataset comprising seismic events processed with more than 40 sensors. The subplots display the stacked distribution of mechanisms across Es/Ep bins (top left), the diamond diagram (top right), the cumulative distribution functions for the filtered data (bottom left), and the resulting confusion matrix, which yields an improved Matthews correlation coefficient (MCC) of 0.59 (bottom right)

Filtering to more than 60 sensors reduces the catalogue to 1,560 events (a 97% decrease). In the stacked plot (Figure 10, top left), the non-shear component below Es/Ep 3 reaches 90% or more, and the diamond diagram (top right) shows good separation. The CDFs (Figure 10, bottom left) show that the accuracy at the operational thresholds is high, about 95% for shear and, for the first time, about 90% for non-shear MTI classed events. These gains raise the MCC to 0.73, a strong correlation, confirming that for this dataset and network geometry the Es:Ep ratio can serve as an accurate proxy for the MTI mechanisms, albeit at severe cost to data volume.

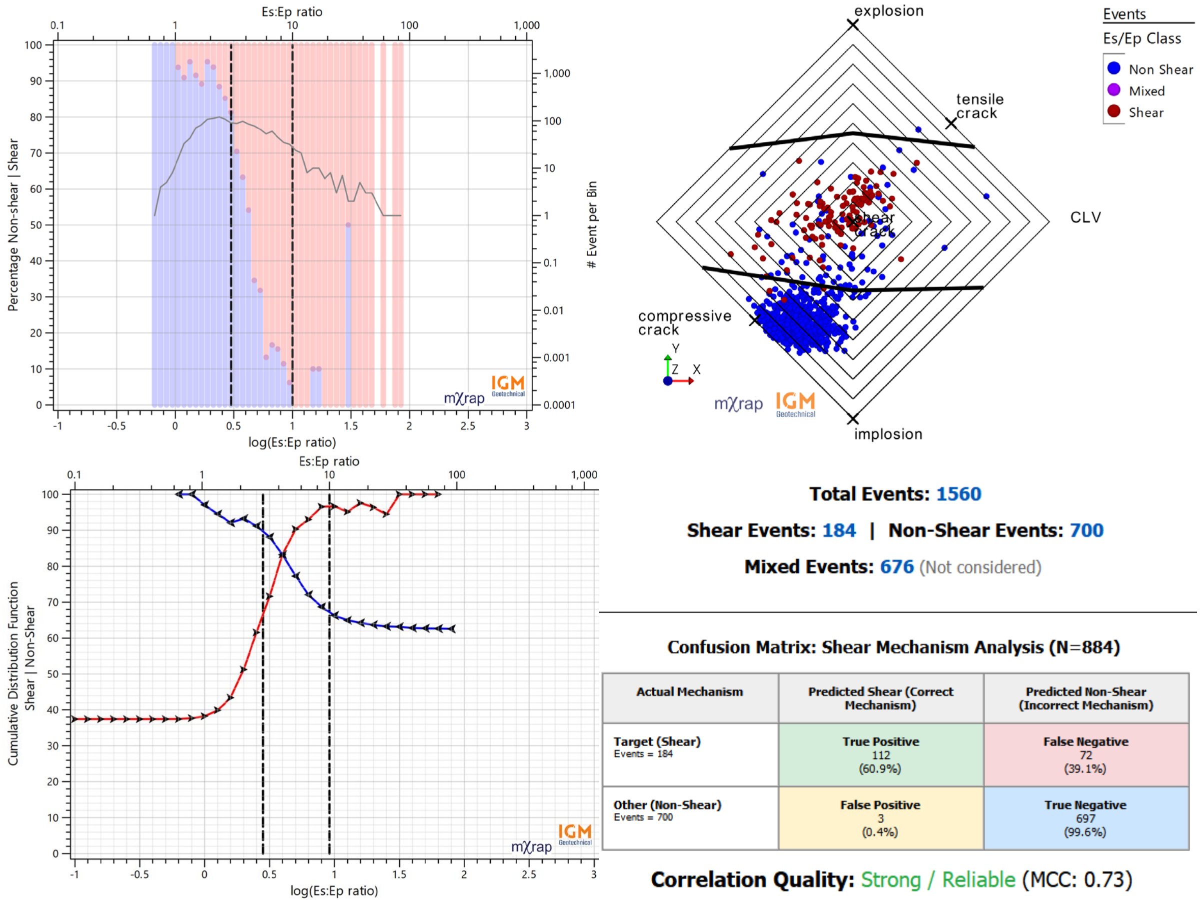

Figure 10 Evaluation of the filtered dataset comprising seismic events processed with more than 60 sensors. The subplots display the stacked distribution of mechanisms across Es/Ep bins (top left), the diamond diagram (top right), the cumulative distribution functions for the filtered data (bottom left), and the resulting confusion matrix, which yields an improved Matthews correlation coefficient (MCC) of 0.73 (bottom right)

Table 3 summarises the results for the different sensors used analyses, giving an overview of the correlation quality and the amount of database reduction due to the required sensors used filter.

Table 3 Summary of results as minimum sensors used is increased

Minimum sensors used	Total number of events considered	Number of shear events considered	Number of non-shear events considered	Number of mixed events considered	Matthews correlation coefficient
Baseline	64,925 (100%)	25,538 (100%)	9,239 (100%)	30,148 (100%)	0.22 (100%)
20+	11,155 (17.2%)	3,313 (13.0%)	2,761 (29.9%)	5,081 (16.9%)	0.36 (164%)
40+	3,700 (5.7%)	661 (2.6%)	1,347 (14.6%)	1,692 (5.6%)	0.59 (268%)
60+	1,560 (2.4%)	184 (0.7%)	700 (7.6%)	676 (2.2%)	0.73 (332%)

4.3 Optimising the usefulness of Es/Ep

This section aims to optimise the baseline dataset to achieve the most effective operational balance. The optimisation process focuses on 2 primary objectives: maximising the total number of usable events and ensuring a minimum acceptable classification correlation level is maintained, quantified here by the MCC. To achieve these outcomes, 2 key parameters are systematically adjusted:

- Es/Ep threshold limits: calibrating the empirical boundaries to safely classify more data. For instance, adjusting the lower non-shear limit of 3 to 4 could help recapture a portion of the 'mixed' events, which currently constitute approximately 50% of the baseline catalogue.
- Minimum sensors used: adjusting the sensor count requirement, as this factor exerts a strong control over data retention.

This methodological approach is useful for practitioners, providing a framework for mining operations to calibrate and maximise the utility of their specific Es/Ep. However, the optimal thresholds generated in this study are strictly site-calibrated values and are not necessarily transferable to other mining environments.

To systematically determine the optimal parameter combination, the MCC was calculated across the entire solution space (defined in Table 2) for the non-shear Es/Ep threshold, the shear Es/Ep threshold, and the minimum number of used sensors. Visualising the data in this manner allows practitioners to identify the specific threshold limits that maximise the total volume of retained events while maintaining a target MCC value. Figure 11 presents this as 4 panels, one for each sensor filter from the previous section (the unfiltered baseline, 20+, 40+, and 60+ sensors). Within each panel, the colour gives the MCC for every combination of the non-shear and shear thresholds, so the best-performing threshold pair is the green region of highest MCC, read off the 2 axes. Comparing the panels shows how that optimum shifts as more sensors are required.

By extracting the optimal limits directly from these specific solution spaces, prioritising the maximum possible event count while targeting a strong predictive correlation (MCC > 0.7), we obtain the following operational results for each sensor cut:

- Baseline (no sensor filter): the absolute maximum MCC achievable is only 0.46, falling short of a strong correlation. Reaching even this moderate level requires extreme thresholds of non-shear Es/Ep < 0.15 and shear Es/Ep > 500. Out of 64,925 total events, this isolates a mere 40 usable events (25 shear, 15 non-shear) and discards 64,885 as mixed. The resulting shear-to-non-shear ratio is 1.67.
- 20+ sensors used: to achieve an MCC > 0.7, the optimal thresholds are non-shear Es/Ep < 0.45 and shear Es/Ep > 50. From the 11,155 available events, this retains only 45 usable classifications (34 shear, 11 non-shear), leaving 11,110 discarded as mixed. The shear-to-non-shear ratio is 3.09.
- 40+ sensors used: with a higher proportion of well-constrained MTI solutions, achieving an MCC > 0.7 allows for thresholds of non-shear Es/Ep < 0.40 and shear Es/Ep > 5.5. This improvement in the required shear threshold retains 2,335 usable events (969 shear, 1,366 non-shear) out of 3,700, leaving 1,365 as mixed. The dataset becomes much more balanced, with a ratio of 0.71.
- 60+ sensors used: at this high trigger-sensor count, achieving an MCC > 0.7 allows the thresholds to converge: non-shear Es/Ep < 3.5 and shear Es/Ep > 4.5. This tight boundary retains 1,377 usable events (484 shear, 893 non-shear) out of the 1,560 total, discarding only 183 events into the narrow-mixed zone. The shear-to-non-shear ratio here is 0.54.

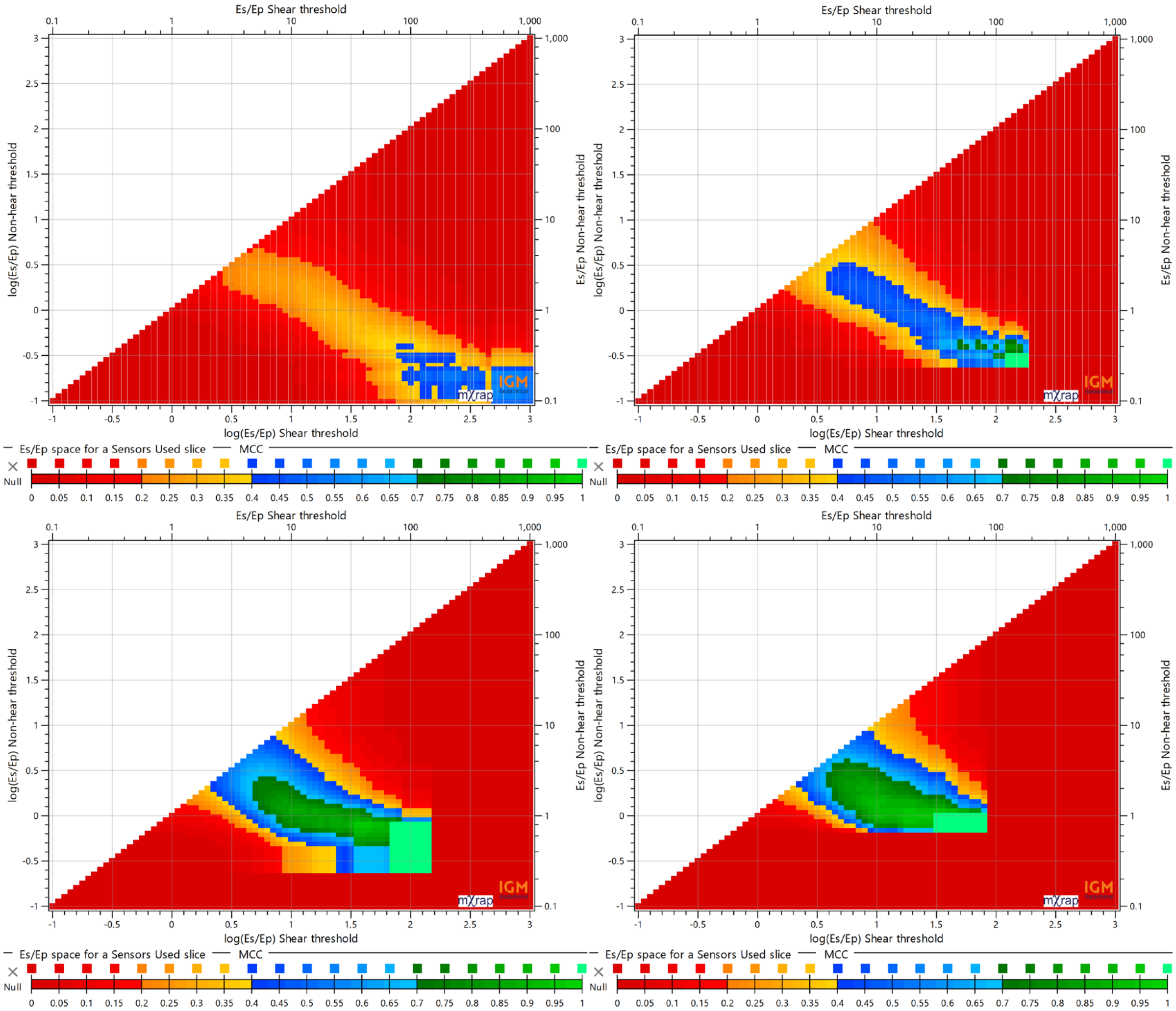

Figure 11 **Matthews correlation coefficient (MCC) solution spaces across combinations of the non-shear Es/Ep threshold (y-axis) and the shear Es/Ep threshold (x-axis); colour indicates the MCC, increasing from red at low values (no correlation) to green at high values (strong correlation), with the white region marking invalid threshold pairs (non-shear ≥ shear). The 4 panels correspond to progressively stricter sensor filters: the unfiltered baseline (top left), 20+ sensors (top right), 40+ sensors (bottom left), and 60+ sensors (bottom right)**

When evaluating the database as a whole to find the optimal balance across all variables, specifically targeting the maximum number of usable events while strictly maintaining a strong predictive correlation (MCC > 0.7), the ideal minimum sensors used requirement is identified as 37 sensors, with the optimal limits for non-shear Es/Ep < 2.25 and shear Es/Ep > 5. As illustrated in Figure 12, out of the 4,253 total events that meet this 37-sensor requirement, this configuration successfully retains 2,636 usable classifications (1,465 shear, 1,171 non-shear) and discards 1,617 events into the mixed zone. This global optimum provides a balanced, reliable dataset with a shear-to-non-shear ratio of 1.25.

Unfortunately, out of the original 64,925 events, only 2,636 are retained as usable classifications. This equates to capturing approximately 4.1% of the baseline catalogue, a retention rate that is very low for routine rock mass analysis, and therefore is not that useful day-to-day. Although the total number of retained events could theoretically be improved by decreasing the target MCC threshold, such a compromise is counterproductive. The primary objective is to identify parameter combinations where empirical Es/Ep values can reliably and confidently predict the likely MTI mechanism for a single event.

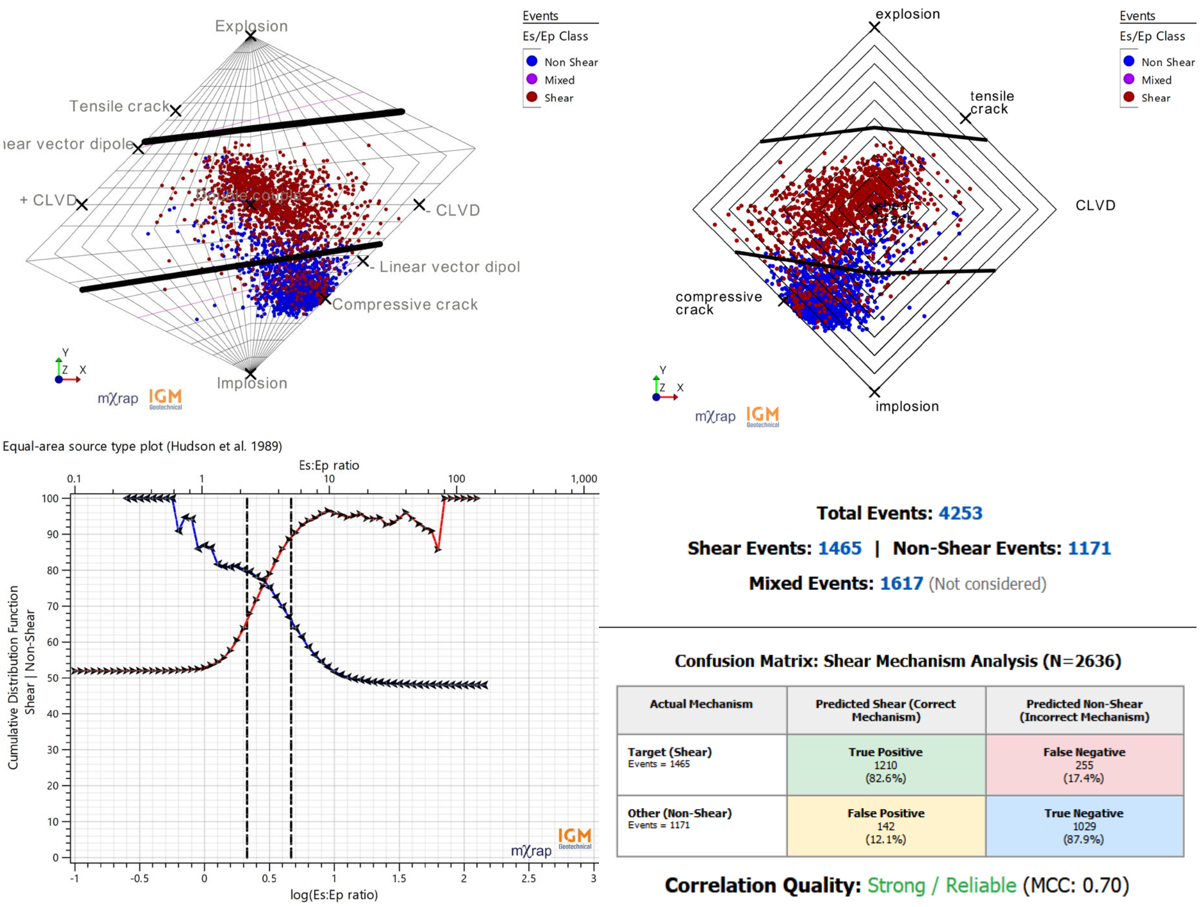

Figure 12 Evaluation of the optimised dataset comprising seismic events processed with more than 37 sensors, applying adjusted empirical thresholds of Es/Ep > 5 for shear and Es/Ep < 2.25 for non-shear classifications. The subplots display the Hudson source-type diagram (top left), the diamond source-type diagram (top right), the cumulative distribution functions for the filtered data (bottom left), and the resulting confusion matrix, which yields a strong Matthews correlation coefficient (MCC) of 0.7 (bottom right)

5 Discussion

5.1 Study assumptions

The conclusions of this study rest on the following assumptions:

1. The dataset is from a single block cave operation, processed by one service provider's automated MTI algorithm. Conclusions apply to this dataset, this network geometry, and this processing chain.
2. Automated MTI solutions are taken as the working reference (ground truth) against which Es/Ep is tested. Errors in the automation are assumed to be systematic, not random.
3. Es/Ep input values were screened; events with Es/Ep = 1.0 (the service provider's flag for unresolved Es or Ep) were assessed and found to have minimal impact on the results.
4. MTI solution quality, including waveform fidelity, signal-to-noise ratio, and focal sphere coverage, was not verified for this catalogue. Database-level deviations would surface as anomalies in the results.
5. The sensors used count is used as the proxy for solution stability. It does not control for sensor position relative to the event, focal sphere coverage, or path effects.
6. Shear and non-shear partitions follow Rigby (2024).

A consequence of using automated MTI as the reference is that this study measures the agreement between 2 coverage-dependent estimators, not the performance of Es/Ep against an absolute truth. The analysis is still informative: MTI uses far more of the recorded waveform than a single scalar ratio and decomposes the source explicitly, so it remains the better estimator, and the systematic-error assumption means relative comparisons between sensor cuts still hold. The results should be read as conditional on the MTI being the more reliable of the 2.

5.2 Discussion of database limitations

In the previous section, the optimisation process revealed a severe operational limitation: achieving a reliable predictive correlation requires discarding most of the dataset. To understand the drivers behind this poor result, this section evaluates the parameter solution spaces. Mapping the classification confidence levels across the data provides the most natural and empirical method to diagnose these underlying issues and understand why the usable data volume is so constrained.

To determine the optimal use of the Es:Ep ratio and investigate this drop-off in data retention, Figure 13 visualises the cumulative solution spaces for both non-shear (Figure 13a) and shear (Figure 13b) mechanisms across all possible combinations of Es/Ep thresholds and used sensors. These solution spaces are cumulative; for any given point on the plot, the classification confidence is calculated using all events that meet or exceed that minimum sensor requirement and fall either below the designated Es/Ep limit (for non-shear) or above it (for shear). Plotting the spaces in this manner is highly advantageous because it allows us to separately evaluate the performance of the shear and non-shear Es/Ep thresholds. This evaluation is useful for diagnostic purposes, as it helps clarify whether the poor baseline correlation is driven by the failure of one specific threshold limit, or if the underlying issues are far more complex. For example, by examining the cumulative non-shear confidence space, one can rapidly determine that applying a filter of 60 or more sensors coupled with an Es/Ep < 3 threshold yields a predictive confidence just above 90%.

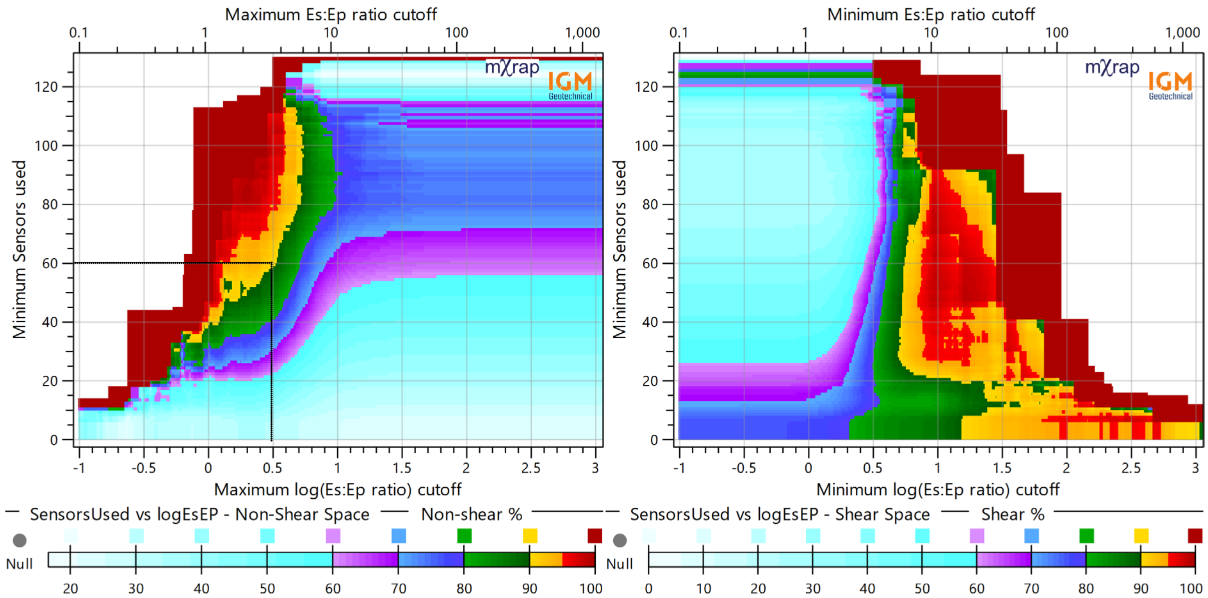

(a) (b)

Figure 13 Cumulative parameter optimisation spaces based on historical data performance, illustrating the relationship between the Es:Ep ratio, the number of used sensors, and classification confidence. The plots display the classification correlation spaces for (a) non-shear and (b) shear mechanisms across all combinations of Es/Ep thresholds and used sensor counts

The primary factor limiting the total volume of usable data is the strict minimum sensor requirement (Figure 13a). Evaluating these confidence spaces reveals an asymmetry in how sensor counts govern predictive reliability for shear versus non-shear mechanisms. For shear events (Figure 13b), a 90% confidence level is achievable at very low sensor counts, provided the Es:Ep ratio is high (e.g. Es/Ep > 20). As the network density increases to 20 or more sensors, this boundary naturally relaxes to lower values of Es/Ep in this case greater than 6. Conversely, non-shear events exhibit no such flexibility. High predictive confidence (90%+) for non-shear mechanisms (Figure 13a) cannot be achieved at lower sensor counts; a strict minimum of at least 35 sensors is required regardless of how low the Es:Ep ratio drops. This non-shear sensor floor is what produces the 37-sensor global optimum reported earlier. Below that count, non-shear events cannot be classified with 90% confidence at any Es/Ep value, which sets the limit for the dataset.

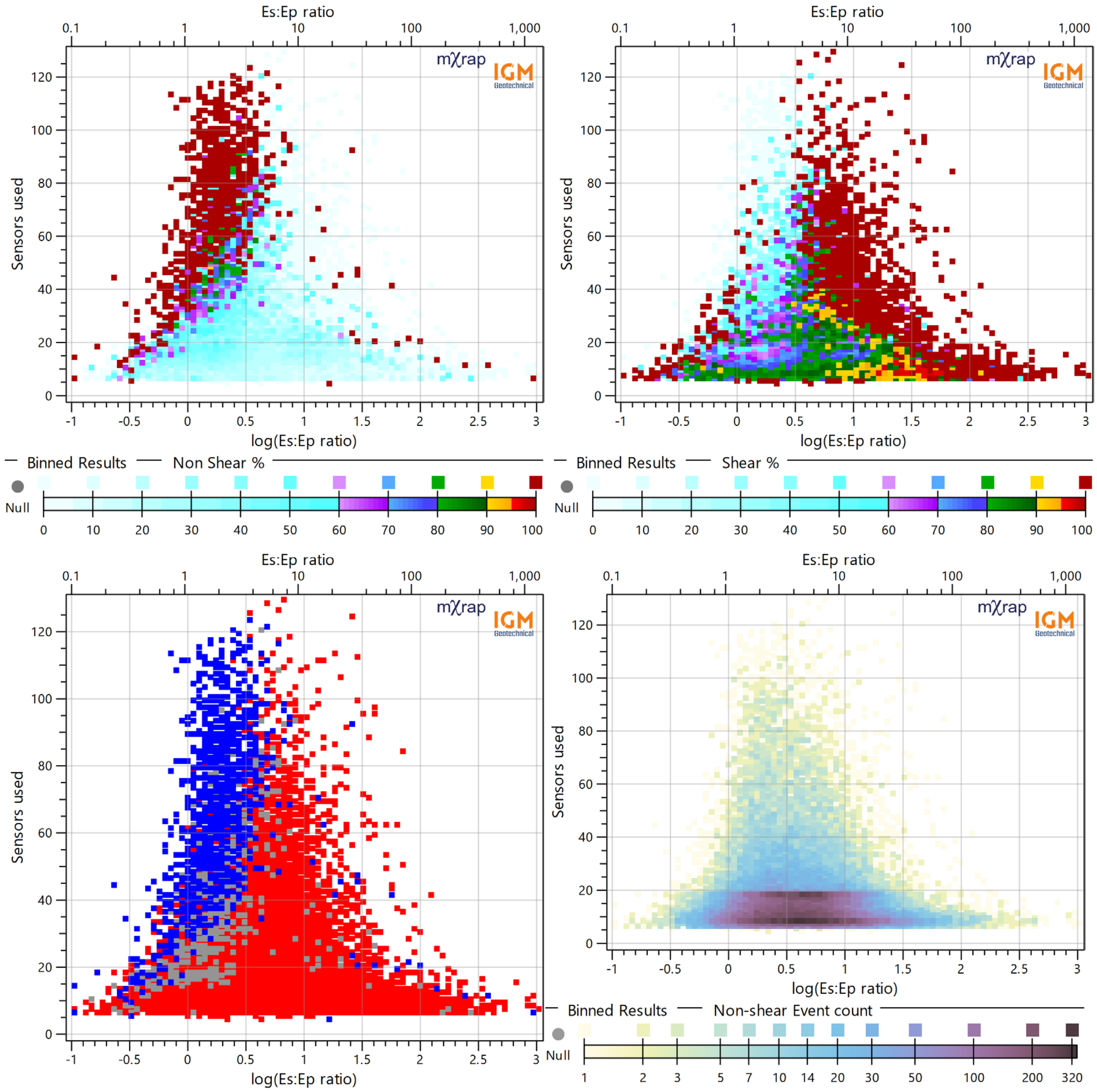

Figure 14 2D binned spatial analysis evaluating the dataset's performance across combinations of the Es:Ep ratio and the number of used sensors. The upper subplots display the calculated classification confidence levels within each bin for moment tensor inversion defined non-shear (top left) and shear (top right) mechanisms. The bottom left subplot categorises individual bins by their statistically dominant mechanism, with red indicating shear, blue indicating non-shear, and grey denoting an unclear classification. The bottom right subplot illustrates the total event count within each corresponding bin, highlighting data density

To better understand the fundamental drivers behind this severe non-shear data constraint and the poor retention results, the dataset must be examined without the influence of cumulative smoothing. Unlike the operational boundaries created in Figure 13, the 2D binned analysis in Figure 14 provides a discrete, 'pixellated' view of the parameter space. This raw spatial resolution helps uncover the underlying features of the dataset much more clearly. In this plot, a bin is assigned a dominant mechanism only if more than 60% of the events within it align with a specific MTI class. If neither mechanism reaches this 60% threshold, the bin is denoted as unclear (grey).

Examining the top row of Figure 14 is immediately apparent; when observing data processed with fewer than 20 sensors, the MTI shear classification overpowers the dataset across almost the entire spectrum of Es:Ep ratios, including values well below the non-shear threshold.

Shear-driven fault slip mechanisms typically generate larger magnitude events that radiate energy over greater distances, thereby naturally triggering a higher number of sensors. Conversely, non-shear mechanisms, such as localised tensile cracking or crushing immediately surrounding excavations, in our experience, are generally smaller in magnitude and energy release, although this can vary by site, meaning they should dictate the lower sensor counts. The parameter space involving fewer than 20 sensors (Figure 14 bottom left) is precisely where the non-shear events should be the most prominent. Instead, this expected physical reality is different. This contradiction raises the possibility that the dominant presence of shear at low sensor counts may not be a true reflection of actual rock mass behaviour and may instead reflect a bias in the automated MTI processing algorithms. The improvement in correlation as the filter tightens is very likely the result of retaining both more reliable MTI and Es/Ep values, by removing poor-quality data. The aim, though, is not to just filter until the correlation is good, but to retain as many events as possible at good correlation. Few operations run seismic networks large enough to record many seismic events with 40 or more sensors, so reducing this requirement as much as possible is important if the Es:Ep ratio is to keep the diagnostic role it still has.

The difficulty in optimising the Es/Ep classification for this database was unexpected and prompts several observations regarding the dataset's behaviour:

- Persistent shear dominance: MTI-defined shear events heavily bias the baseline catalogue, dominating the mechanism distribution, almost 80% of all events are MTI Shear mechanism events.
- The physical anomaly of asymmetric sensor requirements: the discrete bins confirm the stark asymmetry observed in Figure 14. High confidence in shear mechanisms (>60% dominance) is readily achieved with very few sensors, while the non-shear space requires a minimum of 20+ sensors just to establish non-shear dominant bins.
- Few tensile mechanisms resolved: In a block cave, tensile events are expected. The mechanism plots in Figures 8 to 10 show almost no tensile events; even in Figure 8, which retains events recorded by more than 20 sensors, only 6 events are classed as tensile. As the automated MTI attempts a solution for every event it can, this near absence among recorded events is unexpected and points to a limitation in the automated MTI process rather than a true absence of tensile failure.

At this stage, the specific drivers behind these outcomes remain unclear. To resolve these discrepancies, future work will have to systematically investigate the data to evaluate 3 primary hypotheses:

- Automated MTI data quality: Are there systemic quality issues or algorithmic biases within the automated MTI process? Should solutions below a certain quality be removed from the database?
- Spatial biases in the Es/Ep space: Are the calculated Es/Ep values being artificially biased by the specific spatial locations of the sensors relative to the seismic radiation zones?
- Calculation methodology: Is the current method by which the Es/Ep parameter is calculated contributing to these skewed distributions?

Finally, the solution spaces presented in Figure 13 offer an immediate, useful application for routine operational analysis. These plots explicitly map confidence levels as a combined function of the Es:Ep ratio and sensor count, they can be used to assign a 'calibrated confidence' score to any individual seismic event. By cross-referencing an event's specific parameter combination against this historical record, the geotechnical team can gauge the reliability of the empirical prediction. For example, an event recorded by a high number of sensors exhibiting a high Es:Ep ratio indicates a shear mechanism with near certainty in this dataset. Conversely, events falling into lower-confidence zones serve as a built-in warning system. Calculating and appending this calibrated confidence metric across the entire catalogue prompts practitioners to exercise necessary caution, preventing the potentially dangerous assumption that a mechanism is correctly identified based solely on its raw Es/Ep value.

6 Conclusions

This study set out to evaluate the operational validity of the Es:Ep ratio as a diagnostic proxy for seismic source mechanisms in a densely instrumented seismic block cave mine. The baseline statistical analysis revealed that when applied blindly across the full catalogue, the standard empirical thresholds (Es/Ep < 3 for non-shear and > 10 for shear) yielded a poor predictive correlation against MTI ground truth data, resulting in a MCC of 0.22. This confirms the conclusions of Morkel et al. (2019), demonstrating that the parameter is generally unreliable for routine, single event analysis without strict constraints. However, this work also demonstrates that while these standard empirical boundaries are generally in the right ballpark, the predictive quality of the data can be improved by calibrating these thresholds against automated MTI results to suit site-specific conditions.

The predictive accuracy of the Es:Ep ratio is highly dependent on the spatial coverage and density of the recording network, represented in this study by the number of sensors used. This paper has discussed and demonstrated how the Es/Ep parameter can be systematically optimised based to ensure high predictive quality while maximising the usable database size. Mapping classification confidence across the parameter space allows practitioners to assign a calibrated confidence score to individual events, providing a built-in warning system against incorrect mechanism assignment that could mislead ground-control decisions.

Challenges remain. Even in a densely instrumented caving environment, only about 4.1% of the catalogue met the sensor count and Es/Ep thresholds required for confident single event classification. The remaining ~95% had to be excluded. While the study shows that the Es:Ep ratio is operationally valid under specific conditions, its utility remains limited.

The primary driver behind the low retention rate is the persistent dominance of MTI shear events plotting at low Es/Ep values. From our experience, this dominance is concentrated at low sensor counts, which suppresses the expected non-shear result in the parameter space where smaller, local tensile and compressive cracking events would normally be expected. To restore operational trust in the Es/Ep parameter and increase the volume of usable data, these discrepancies must be resolved.

Further work should first apply the tools presented here to predominantly manually processed catalogues. This would help establish whether the anomalies are driven by systemic biases in the automated MTI processing, by spatial biases in how the sensors sample the seismic radiation pattern, or by limitations in how the event Es:Ep ratio is calculated.

Use of artificial intelligence disclosure statement

In the preparation of this work, the author used Ollama (2026) for suggestions on improving the structure, language and grammar of the paper. The author has reviewed the content and edited it where required and take full responsibility for said content.

References

Abolfazlzadeh, Y, Smith-Bougher, L, Anderson, Z, Jalbout, A & Mataseje, A 2019, 'Calibration of a seismic hazard assessment tool using velocity fields and geotechnical data', in J Wesseloo (ed.), *MGR 2019: Proceedings of the First International Conference on Mining Geomechanical Risk*, Australian Centre for Geomechanics, Perth, pp. 233–244, https://doi.org/10.36487/ACG_rep/1905_12_Abolfazlzadeh

Boatwright, J & Fletcher, JB 1984, 'The partition of radiated energy between P and S waves', *Bulletin of the Seismological Society of America*, vol. 74, no. 2, pp. 361–376.

Cai, M, Kaiser, PK & Martin, CD 1998, 'A tensile model for the interpretation of microseismic events near underground openings', *Seismicity Caused by Mines, Fluid Injections, Reservoirs, and Oil Extraction*, Springer.

Fawcett, T 2006, 'An introduction to ROC analysis', *Pattern Recognition Letters*, vol. 27, no. 8, pp. 861–874.

Gibowicz, S, Young, R, Talebi, S & Rawlence, D 1991, 'Source parameters of seismic events at the Underground Research Laboratory in Manitoba, Canada: scaling relations for events with moment magnitude smaller than -2', B*ulletin of the Seismological Society of America*, vol. 81, no. 4, pp. 1157–1182.

Gibowicz, SJ & Kijko, A 1994, An introduction to mining seismology, *Academic Press, Inc*, San Diego.

Hudson, JA, Pearce, RG & Rogers, RM 1989, 'Source type plot for inversion of the moment tensor', Journal of Geophysical Research, vol. 94, no. B1, pp. 765–774.

Hudyma, M & Potvin, YH 2010, 'An engineering approach to seismic risk management in hardrock mines', *Rock Mechanics and Rock Engineering*, vol. 43, no. 6, pp. 891–906.

Ma, J, Dineva, S, Cesca, S & Heimann, S 2018, 'Moment tensor inversion with three-dimensional sensor configuration of mining induced seismicity (Kiruna mine, Sweden)', *Geophysical Journal International*, vol. 213, no. 3, pp. 2147–2160.

Matthews, B 1975, 'Comparison of the predicted and observed secondary structure of T4 phage lysozyme', *Biochim Biophys Acta*, vol. 405, no. 2, pp. 442–451.

Mendecki, AJ 2013, 'Mine seismology: glossary of selected terms', in A Malovichko & D Malovichko (eds), *Proceedings of Eighth International Symposium on Rockbursts and Seismicity in Mines, RaSiM8*, Geophysical Survey of Russian Academy of Sciences, pp. 527–551.

Morkel, IG & Wesseloo, J 2017, 'A technique to determine systematic shifts in microseismic databases', in J Wesseloo (ed.), *Deep Mining 2017: Proceedings of the Eighth International Conference on Deep and High Stress Mining*, Australian Centre for Geomechanics, Perth, pp. 105–116, https://doi.org/10.36487/ACG_rep/1704_05_Morkel

Morkel, IG, Wesseloo, J & Harris, P 2015, 'Highlighting and quantifying seismic data quality concerns', in PM Dight (ed.), *FMGM 2015: Proceedings of the Ninth Symposium on Field Measurements in Geomechanics*, Australian Centre for Geomechanics, Perth, pp. 539–549, https://doi.org/10.36487/ACG_rep/1508_37_Morkel

Morkel, IG, Wesseloo, J & Potvin, Y 2019, 'The validity of Es/Ep as a source parameter in mining seismology', in W Joughin (ed.), *Deep Mining 2019: Proceedings of the Ninth International Conference on Deep and High Stress Mining*, The Southern African Institute of Mining and Metallurgy, Johannesburg, pp. 385–398, https://doi.org/10.36487/ACG_rep/1952_29_Morkel

Reyes-Montes, JM, Sainsbury, BL, Pettitt, WS, Pierce, M & Young, RP 2010, 'Microseismic tools for the analysis of the interaction between open pit and underground developments', in Y Potvin (ed.), *Caving 2010: Proceedings of the Second International Symposium on Block and Sublevel Caving*, Australian Centre for Geomechanics, Perth, pp. 119–131, https://doi.org/10.36487/ACG_rep/1002_5_Reyes-Montes

Rigby, A 2024, 'Physically motivated moment-tensor decomposition for mining-induced seismicity', *Geophysical Journal International*, vol. 236, pp. 443–455.

Sato, T 1978, 'A note on body wave radiation from expanding tension crack', *Journal of Physics of the Earth*, vol. 26, no. 3, pp. 245–255.

Sweby, G, Trifu, C, Goodchild, D & Morris, L 2006, 'High resolution seismic monitoring at Mt Keith open pit mine', *Proceedings of Golden Rocks 2006, 41st U.S. Symposium on Rock Mechanics (USRMS)*, American Rock Mechanics Association, Alexandria.

Vavryčuk, V 2015, 'Moment tensor decompositions revisited', *Journal of Seismology*, vol. 19, pp. 231–252.